Available online at www.sciencedirect.com
ScienceDirect
Applied Catalysis B: Environmental 83 (2008) 78–84
APPLIED CATALYSIS B: ENVIRONMENTAL
www.elsevier.com/locate/apcatb

Highly active $La_2O_3/Ti_{1-x}B_xO_2$ visible light photocatalysts prepared under supercritical conditions

Yuning Huo, Xinyu Zhang, Yi Jin, Jian Zhu, Hexing Li *

Department of Chemistry, Shanghai Normal University, Shanghai 200234, China

Received 19 October 2007; received in revised form 31 January 2008; accepted 6 February 2008
Available online 14 February 2008

Abstract

$La_2O_3/Ti_{1-x}B_xO_2$ nanocrystals are prepared under supercritical conditions in which the La_2O_3 is present in a separate phase adsorbed by TiO_2 while B-dopants are incorporated into TiO_2 lattice via Ti–O–B bond. During degradation of methylene blue under visible irradiation, the as-prepared photocatalyst exhibits higher activity than the undoped TiO_2, the La_2O_3/TiO_2, the $Ti_{1-x}B_xO_2$, and even the $La_2O_3/Ti_{1-x}B_xO_2$ obtained via direct calcinations, showing synergetic promoting effects from the supercritical treatment, the La_2O_3 and the B-dopant. The B-doping extends light absorbance to visible region while the La_2O_3 could enhance the surface area and also capture the photoelectrons, leading to the lower recombination between photoelectrons and holes. Supercritical treatment results in well-crystallized anatase and high surface area, which facilitate the light absorbance, the adsorption of organic substrate, and the separation of photoelectrons from holes, leading to the enhanced quantum yield. Meanwhile, supercritical treatment may strengthen the interactions of the La_2O_3 and the B-dopants with TiO_2, leading to enhanced promoting effects.

Keywords: $La_2O_3/Ti_{1-x}B_xO_2$; Synergetic effect; Supercritical treatment; Visible-light photocatalysis

1. Introduction

Photocatalysis has caused intensive attention both in dealing with the environmental pollution from photodegradation and in producing new energy from photosplit of water [1–3]. Among various oxide semiconductors, the TiO_2 photocatalyst has been most thoroughly investigated owing to its cheapness, non-toxicity, and structural stability [4–6]. However, besides low quantum efficiency, the pure TiO_2 photocatalyst could be activated only by UV lights due to its large energy band gap (~3.2 eV) [7,8], which greatly limits its practical application since the availability of ultraviolet (UV) lights in solar light is only less than 3–5%. Therefore, a great number of attempts have been made to enhance the photocatalytic efficiency and extend the spectral response to visible region by doping TiO_2 with metals [9–12] metallic ions and oxides [13–15] nonmetal-dopants [16–19] and organic photosensitizers [20–24]. Up to now, nearly all the doped TiO_2 photocatalysts are prepared by sol–gel method, followed by calcinations to remove organic species. However, calcination at high temperature usually causes particle agglomeration and pore collapse, leading to the low surface area and the poor dispersion of the dopants in the TiO_2 network, corresponding to lower photocatalytic activity [25,26]. Previously, we reported a variety of TiO_2 photocatalysts doped with metal oxides and nonmetal additives prepared under supercritical conditions [27–30]. In comparison with the normal solvothermal conditions, the supercritical conditions with ethanol fluid exhibit higher pressure and temperature (ca. 553 K and 13.5 MPa) which could enhance the crystallization degree and the doping effect on TiO_2. Meanwhile, the organic species in the TiO_2-based sample could be extracted and the sample could be dried directly due to the absence of surface tension under supercritical conditions, leading to the high surface area since the porous structure in the precursor is reserved. Previous results demonstrated that doping TiO_2 with nonmetal-dopants could extend light absorbance to visible region [16,18,28], while the presence of metal oxides could enhance quantum efficiency and thermal stability of anatase phase [13,24], which stimulates us to synthesize the TiO_2 co-doped with both the metal oxide and the

* Corresponding author. Tel.: +86 21 64322272; fax: +86 21 64322272.
E-mail address: HeXing-Li@shnu.edu.cn (H. Li).

0926-3373/$ – see front matter © 2008 Elsevier B.V. All rights reserved.
doi:10.1016/j.apcatb.2008.02.005

nonmetal-dopant. Herein, we report a new $La_2O_3/Ti_{1-x}B_xO_2$ photocatalyst with the aim to examine the synergetic promoting effects of the La_2O_3 and the B-dopant as well as the supercritical treatment. The B-doped TiO_2 has been seldom studied since, unlike other nonmetal-dopants (e.g. N, S, F, etc.), the B-dopants are difficult to be incorporated into the TiO_2 lattice via regular methods (e.g., sol–gel method). The supercritical treatment supplies a powerful way to incorporate B-dopants in the TiO_2 lattice which might induce unusual structural modification. In comparison with other metal oxides including the other rare earth element oxides, the La_2O_3 is cheap and easily available, especially in China. Besides, the presence of La_2O_3 could greatly enhance the surface area and also stabilize the anatase of TiO_2 against transformation to rutile [31]. The as-prepared $La_2O_3/Ti_{1-x}B_xO_2$ displays high activity during photodegradation of methylene blue under visible irradiation and the correlation of the catalytic performance to the structural characteristics is discussed based on detailed characterizations.

2. Experimental methods

2.1. Catalyst preparation

A solution containing 10 ml EtOH, 2.5 ml 1.0 M HNO_3, and desired amount of $La(NO_3)_3$ and H_3BO_3 is added dropwise into a solution comprised of 10 ml $Ti(O–C_4H_9)_4$ and 40 ml EtOH at 313 K under vigorous stirring and kept stirring continuously until the formation of TiO_2 xerogel. The TiO_2 xerogel is transferred into a 500 ml autoclave containing 250 ml ethanol solution with trace KBH_4 for supercritical treatment under 553 K and 13.5 MPa. After 2 h, the vapor is released slowly and the system is allowed to cool down to room temperature in the N_2 flow. The as-received solid is washed thoroughly by ethanol solution, followed by calcining at a desired temperature for 8 h to remove the residual solvent and other organic species. Preliminary experiments confirmed that the optimum calcination temperature is 773 K. Finally, the as-prepared sample is crushed and kept in vacuum until the time of use. The La/Ti molar ratio is fixed at 1.2%, which has been proved to be the optimum La-content [32]. The B-content is adjusted by changing the concentration of H_3BO_3 in the mother solution and determined by XPS spectra. The samples with different Ti/B molar ratios are denoted as $La_2O_3/Ti_{1-x}B_xO_2$(SC)-*n*, where SC refers to supercritical treatment and *n* = 1–6 corresponding to different B/Ti molar ratios (see Table 1). The undoped TiO_2(SC), the $Ti_{1-x}B_xO_2$(SC) (B/Ti = 2.2%) and the La_2O_3/TiO_2(SC) (La/Ti = 1.2%) are obtained by changing the composition of the mother solution. For comparison, a $La_2O_3/Ti_{1-x}B_xO_2$(DC) with La/Ti and B/Ti ratios of 1.2% and 2.2% is also prepared by traditional sol–gel method, where DC refers to direct calcinations.

2.2. Catalyst characterization

The structure of the as-prepared samples is determined by X-ray diffraction (XRD, Rigacu Dmax-3C, Cu Kα radiation). The light absorption is measured by UV–visible diffuse reflectance spectra (DRS, MC-2530) and photoluminescence spectra (PLS, Varian Cary-Eclipse 500). The N_2 adsorption–desorption isotherms are obtained at 77 K on a NOVA 4000, from which the surface area (S_{BET}) and the pore volume (V_P) are calculated based on Barret–Joyner–Helena (BJH) method. Transmission electronic morphologies (TEM) and selected area electronic diffractions (SAED) are obtained on a JEM-2010. The surface electronic states are analyzed by X-ray photoelectron spectroscopy (XPS, PerkinElmer PHI 5000C). All the binding energy (BE) values are calibrated by using the standard BE value of contaminant carbon (C_{1s} = 284.6 eV) as a reference. The molar ratios of La/Ti and B/Ti in the samples are determined by using 6.67, 0.13 and 2.001 as the PHI sensitivity factors corresponding to XPS peaks in the $La_{3d5/2}$, B_{1s} and $Ti_{2P3/2}$ levels, respectively [33].

2.3. Activity test

The liquid-phase photocatalytic degradation of methylene blue (MB) is carried out at 303 K in an 80 ml self-designed quartz photochemical reactor containing 0.050 g catalyst and 50 ml 0.010 g/L MB aqueous solution. After being stirred for 1 h which is long enough for the reactant to reach adsorption equilibrium on the photocatalyst (see Figure S1), the photocatalytic reaction is initiated by irradiating the system with three 150 W xenon lamps located at 30 cm away from the

Table 1
Some structural parameters of the undoped and doped TiO_2 samples

Catalyst	La/Ti (%)	B/Ti (%)	S_{BET} (m^2/g)	V_P (cm^3/g)	D_P (nm)	E_g (eV)
P25 TiO_2	0	0	45	0.20	20	3.1
TiO_2(DC)	0	0	7.6	0.010	5.0	3.2
TiO_2(SC)	0	0	84	0.40	20	3.2
La_2O_3/TiO_2(SC)	1.2	0	93	0.45	15	3.2
$Ti_{1-x}B_xO_2$(SC)	0	2.2	110	0.51	24	2.6
$La_2O_3/Ti_{1-x}B_xO_2$(SC)-1	1.2	0.80	112	0.52	20	3.1
$La_2O_3/Ti_{1-x}B_xO_2$(SC)-2	1.2	0.90	129	0.60	21	2.9
$La_2O_3/Ti_{1-x}B_xO_2$(SC)-3	1.2	1.6	131	0.65	23	2.8
$La_2O_3/Ti_{1-x}B_xO_2$(SC)-4	1.2	2.2	143	0.75	24	2.6
$La_2O_3/Ti_{1-x}B_xO_2$(SC)-5	1.2	3.8	145	0.63	24	2.6
$La_2O_3/Ti_{1-x}B_xO_2$(SC)-6	1.2	5.0	140	0.57	23	2.6
$La_2O_3/Ti_{1-x}B_xO_2$(DC)-4	1.2	2.2	23	0.10	7.5	2.9

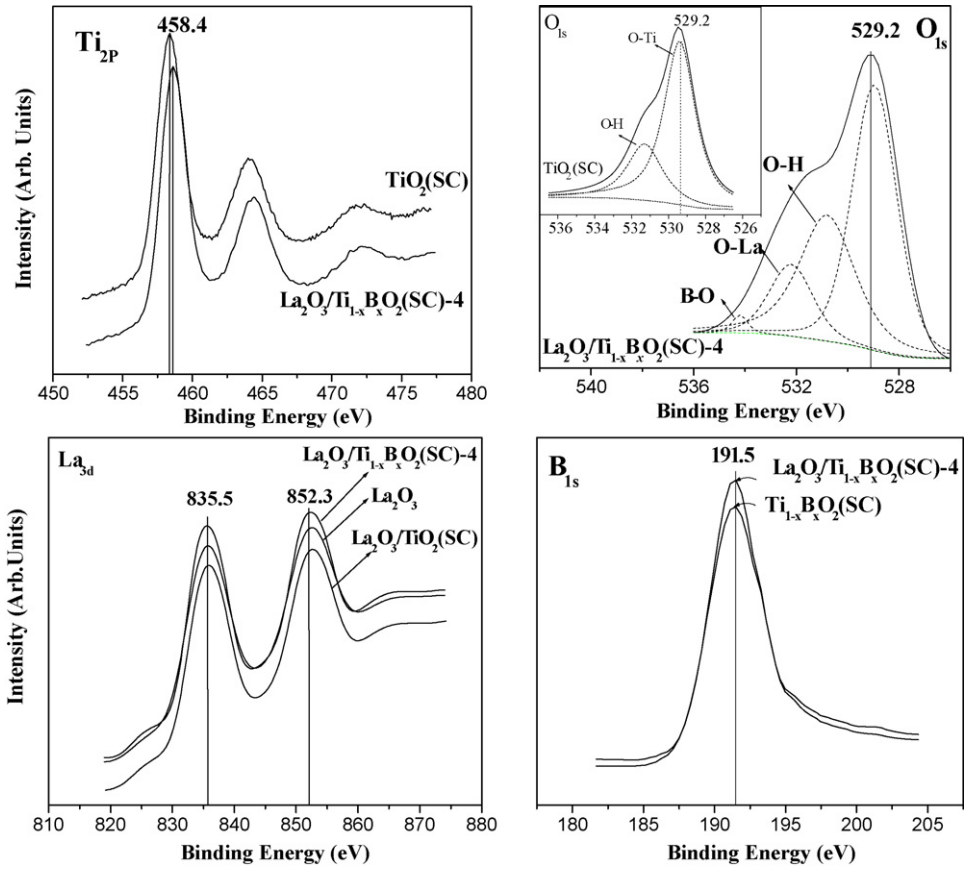

Fig. 1. XPS spectra of different photocatalysts calcined at 773 K.

reaction solution. All the UV light with wavelength less than 420 nm are removed by a glass filter (JB-420, Shanghai Mingshen Chromatic Glass Limited Company). Each run of reactions is lasted for 3 h and the left MB is analyzed by a UV spectrophotometer (UV 7504/PC) at its characteristic wavelength ($\lambda = 665$ nm) to determine the degradation yield [34]. Preliminary tests demonstrate a good linear relationship between the light absorbance and the MB concentration. Only less than 7.0% MB decomposes after reaction for 3 h under the same conditions in the absence of either the photocatalyst or the light irradiation (Figures S1 and S2) and thus, could be neglected in comparison with that obtained from photocatalytic degradation. The reproducibility is checked by repeating the results at least three times and was found to be within acceptable limits (±5%).

3. Results and discussion

3.1. Structural characteristics

The XPS spectra in Fig. 1 demonstrate that the presence of either La_2O_3 and B-dopant has no significant influence on the Ti_{2P} level, implying that neither the Ti–La nor the Ti–B bonding is formed. Only La_2O_3 adsorbed on TiO_2 has been detected, corresponding to the binding energies (BE) of 835.5 and 852.3 eV in the $La_{3d5/2}$ and $La_{3d3/2}$ levels, the same as observed in pure La_2O_3. According to the peak separation, the La_2O_3/TiO_2(SC) exhibits three peaks around 529.0, 531.0 and 532.4 eV in the O_{1S} level, corresponding to the Ti–O, the surface H–O and La–O bonds, respectively [24,26]. The La_2O_3/$Ti_{1-x}B_xO_2$ (SC) exhibits an additional peak at 534.2 eV indicative of the B–O bond [35]. The BE of the B-dopants is determined as 191.5 eV in the B_{1S} level, much lower than that in either the pure B_2O_3 (193.9 eV) or the H_3BO_3 (193.5 eV) [36], indicating that the B-dopants are incorporated into the TiO_2 lattice rather than existing in a separate phase. As the BE of the B-dopant is 3.3 eV higher than that of the pure TiB_2 (188.2 eV) [24], the formation of the O–Ti–B bond is not possible. Considering that the BE of the adsorbed $B_4O_7^{2-}$ is around 192.0 eV [36], it is reasonable to conclude that partial B atoms in the $B_4O_7^{2-}$ are replaced by Ti atoms to form Ti–O–B bond [37] via co-condensation between the $Ti(OH)_4$ and $B(OH)_3$, as described in Scheme 1. Thus, the B-doped TiO_2 is denoted as $Ti_{1-x}B_xO_2$ rather than as $TiO_{2-x}B_x$, which means the formation of the Ti–O–B bonding rather than the O–Ti–B bonding. In comparison with the B–O–B bond, partial electrons transfer from Ti to O and further to B in the Ti–O–B bond owing to the bigger electronegativity of the B than that of the Ti, which could account for the lower BE of both the O and the B in La_2O_3/$Ti_{1-x}B_xO_2$(SC) and $TiO_{2-x}B_x$(SC) samples than those in undoped TiO_2(SC) and pure $B_4O_7^{2-}$. The failure in observing the BE shift of the Ti could be attributed its relatively greater atomic weight comparing to that of either the B or the O atom. The FTIR spectrum (Figure S3) further confirms that, besides

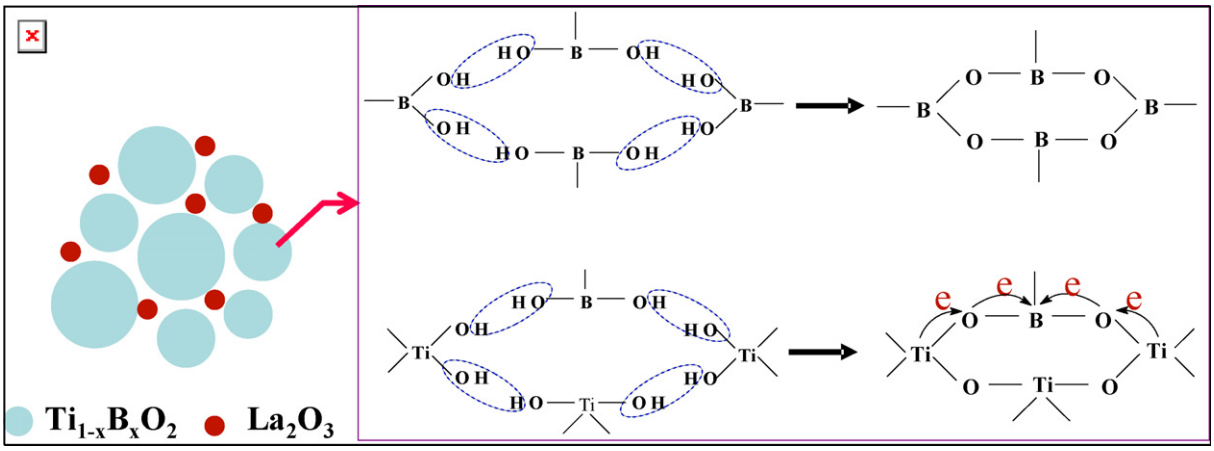

Scheme 1. The formation of the Ti–O–B bond and the electron transfer in the $La_2O_3/Ti_{1-x}B_xO_2$(SC) photocatalyst.

the absorption peaks at 1630/3400, 655 and 510 cm^{-1} indicative of the surface O–H, the Ti–O, and the La–O, respectively [26,38], the $La_2O_3/Ti_{1-x}B_xO_2$ sample also displays an absorbance peak around 1390 cm^{-1}, corresponding to the B–O bonding [37].

As shown in Fig. 2, the XRD patterns reveal that all the TiO_2(SC), La_2O_3/TiO_2(SC), $Ti_{1-x}B_xO_2$(SC), and $La_2O_3/Ti_{1-x}B_xO_2$(SC) samples are present in unique anatase phase after being calcined at 773 K. The $La_2O_3/Ti_{1-x}B_xO_2$(SC) shows higher crystallization degree of anatase than either the $Ti_{1-x}B_xO_2$(SC) or the La_2O_3/TiO_2(SC) owing to synergetic promoting effects from both the La_2O_3 and the B-dopant. No significant difference in the positions of XRD peaks between the La_2O_3/TiO_2(SC) and the TiO_2(SC) has been observed. However, the principal XRD peak of either the $Ti_{1-x}B_xO_2$(SC) or the $La_2O_3/Ti_{1-x}B_xO_2$(SC) shift positively by 0.1° (see the attached patterns). These results further confirm that the La_2O_3 is present in separate phase adsorbed on the TiO_2 while the B-dopants are incorporated into the TiO_2 lattice, leading to the change of TiO_2 crystal parameters [24]. The crystallization degree of anatase increases with the increase of the calcination temperature (Figure S4). Based on the XRD patterns (Figure S4) and our previous results [27,28], the phase transformation temperatures from anatase to rutile for $La_2O_3/Ti_{1-x}B_xO_2$(SC), La_2O_3/TiO_2(SC), $Ti_{1-x}B_xO_2$(SC), TiO_2(SC) and TiO_2(DC) are determined as 1373, 1323, 1073, 973 and 673 K, respectively. The higher transformation temperature of the TiO_2(SC) than that of the TiO_2(DC) demonstrates that the supercritical treatment enhances the thermal stability of anatase. This could be attributed to the porous structure formed under supercritical conditions which might inhibit the migration and the arrangement of Ti and O atoms to form rutile during calcinations [39]. The surface La_2O_3 species could protect the TiO_2 nanoparticles from agglomeration and rearrangement during calcinations which also retards the phase transformation, leading to the enhanced thermal stability of anatase. The promoting effect of the B-doping on thermal stability could be attributed to the incorporation of B-dopants into the TiO_2 lattice via Ti–O–B bonding, resulting in a strong crystal distortion force which could also protect the anatase from phase transformation. The XRD patterns display no significant signals indicative of La_2O_3 phase in either the La_2O_3/TiO_2(SC) or the $La_2O_3/Ti_{1-x}B_xO_2$(SC) even after being calcined at very high temperature, which could be attributed to the low La-content and the high dispersion of La_2O_3.

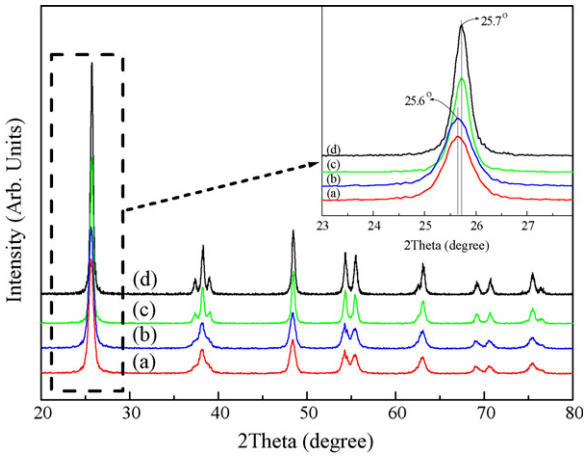

Fig. 2. XRD patterns of the (a) TiO_2(SC), (b) La_2O_3/TiO_2(SC), (c) $Ti_{1-x}B_xO_2$(SC), and (d) $La_2O_3/Ti_{1-x}B_xO_2$(SC)-4 calcined at 773 K.

TEM morphologies (Figure S5) reveal that all the TiO_2(SC), La_2O_3/TiO_2(SC), $Ti_{1-x}B_xO_2$(SC) and $La_2O_3/Ti_{1-x}B_xO_2$(SC) samples calcined at 773 K are present in uniform cubic nanoparticles. The La_2O_3/TiO_2(SC) exhibits higher dispersion than the TiO_2(SC) since the La_2O_3 could act as the support for depositing TiO_2 nanoparticles. The attached SAED image shows high crystallization degree of anatase, which is in good accordance of the cubic crystal cell of anatase (Figure S6).

Other structural parameters are listed in Table 1. All samples obtained under supercritical conditions exhibit much higher S_{BET} and V_p than those obtained via direct calcination since the porous structure in the precursors could be preserved owing to the lack of surface tension under supercritical conditions [40,41]. The presence of La_2O_3 causes a decrease in average pore size (D_P) due to partial blockage of pore channels. Thus, the slight increase in both the S_{BET} and the V_p is mainly attributed to the enhanced particle dispersion. The B-doping

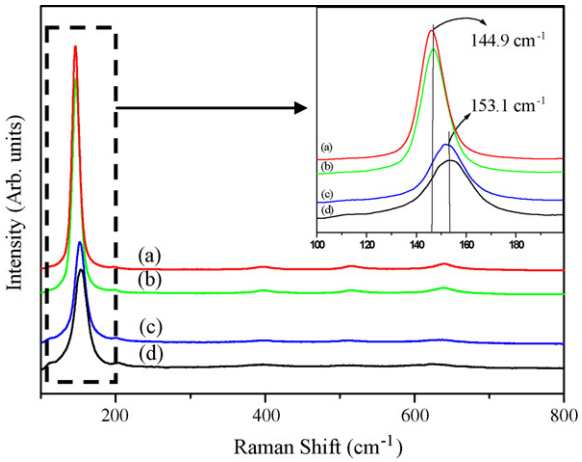

Fig. 3. Raman spectra of (a) TiO_2(SC), (b) La_2O_3/TiO_2(SC), (c) $Ti_{1-x}B_xO_2$(SC), and (d) $La_2O_3/Ti_{1-x}B_xO_2$(SC)-4 calcined at 773 K.

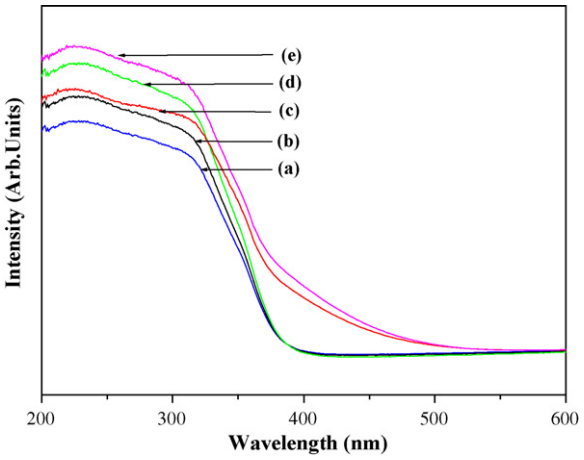

Fig. 4. UV–vis DRS spectra of (a) TiO_2(DC) (b) TiO_2(SC), (c) $Ti_{1-x}B_xO_2$(SC), (d) La_2O_3/TiO_2(SC), and (e) $La_2O_3/Ti_{1-x}B_xO_2$(SC)-4 calcined at 773 K.

causes an abrupt increase in both the S_{BET} and the V_p owing to the incorporation of B-dopants into the TiO_2 lattice via a cage-like model (see Scheme 1), leading to formation of more porous structures.

The Raman spectra (Fig. 3) demonstrate that all the as-prepared samples are present in unique anatase phase. No significant deference between the La_2O_3/TiO_2(SC) and the TiO_2(SC) has been observed. However, both the $Ti_{1-x}B_xO_2$(SC) and the $La_2O_3/Ti_{1-x}B_xO_2$(SC) display positive shift in absorbance position by 8.2 cm^{-1}, suggesting that the B-doping induces more oxygen vacancies and/or crystal defects [9,42]. The oxygen vacancies are resulted from the incorporation of B-dopants into TiO_2 lattice via Ti–O–B bond which may reduce the O/Ti ratio, taking into account that the B-dopant is present in +3 while Ti is present in +4 oxidation state. Meanwhile, the replacement of Ti by B to form the Ti–O–B bond also induces crystal defects since B atom is much smaller than the Ti atom. The PLS spectra (Figure S7) reveal that the absorbance peak corresponding to the emission from band edge free excitation increases after B-doping, which further confirms the increase in oxygen vacancies and/or crystal defects, leading to reduced recombination between photoelectrons and holes since both oxygen vacancies and crystal defects could capture photoelectrons [43]. The presence of La_2O_3 could trap photoelectrons and thus inhibit their recombination with holes, leading to enhanced PLS response.

As shown in Fig. 4, the UV–vis DRS spectra demonstrate that the $La_2O_3/Ti_{1-x}B_xO_2$(SC) exhibits the highest light absorbance efficiency in both UV region and visible region. The supercritical treatment enhances light absorbance owing to the high crystallization degree of anatase, which facilitates the transfer of photoelectrons from the bulk to the surface and thus, could inhibit their recombination with the photoholes [40,41]. Meanwhile, the supercritical treatment could also increase crystal defects which could capture the photoelectrons and thus, inhibit their recombination with photoholes [41]. The presence of La_2O_3 could promote light harvesting because of the enhanced surface area (see Table 1). Meanwhile, similar to Fe_2O_3, the La_2O_3 could capture photoelectrons and inhibit their recombination with holes, which might further enhance light absorbance [32]. As confirmed by the XRD patterns (Fig. 2) and the Raman spectra (Fig. 3), the B-doping induces oxygen vacancies and/or crystal defects [9,42], which could capture the photoelectrons and thus inhibit recombination of photoelectrons and holes, leading to enhanced light absorbance [43]. The B-doping extends light absorbance to visible region owing to the formation of Ti–O–B bonds, which might generate intermediate energy levels [24], leading to a narrower energy band gap. The energy band gaps (E_g) are calculated according to following formula [44,45]:

$$(\alpha h\upsilon)^n = k(h\upsilon - E_g)$$

Plotting $(\alpha h\upsilon)^{1/2}$ vs. $h\upsilon$ (see Figure S8) gives the extrapolated intercept corresponding to the E_g values. As shown in Table 1, either the supercritical treatment and the presence of La_2O_3 has no significant influence on E_g while the B-doping results in abrupt decrease in E_g [24,46]. The E_g decreases gradually with the increase of B-content owing to the increase of Ti–O–B bonds. However, excessive B-content has no significant influence on E_g due to the formation of B_2O_3 separate phase. The $La_2O_3/Ti_{1-x}B_xO_2$(DC) exhibits bigger E_g than the $La_2O_3/Ti_{1-x}B_xO_2$(SC) with the same La/Ti and B/Ti molar ratios since the supercritical treatment could ensure more B-dopants incorporating with TiO_2 lattice to form Ti–O–B bonds and also strengthen the interaction between the B-dopants and the TiO_2, leading to enhanced B-doping effect. This could be confirmed by XPS spectra in B_{1S} level (Figure S9). The $La_2O_3/Ti_{1-x}B_xO_2$(SC) displays one peak around 191.5 eV indicative of the B species incorporated into TiO_2 lattice. However, the $La_2O_3/Ti_{1-x}B_xO_2$(DC) displays a peak with binding energy around 192.0 eV, suggesting the presence of adsorbed boron oxide species [36].

3.2. Catalytic performance

During liquid phase photocatalytic degradation of MB under visible irradiation (>420 nm), the activity of $La_2O_3/Ti_{1-x}B_xO_2$(SC)-4 first increases and then decreases with the increase

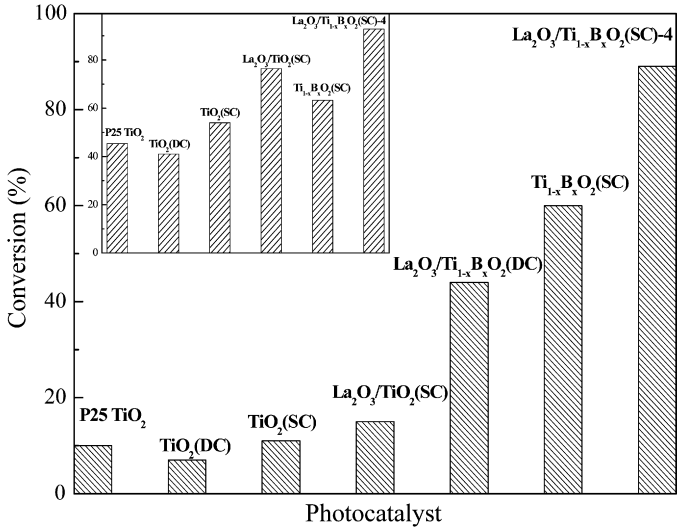

Fig. 5. Activities of different photocatalysts for MB degradation under visible irradiation. Reaction conditions: 0.050 g catalyst, 50 ml 0.010 g/l MB, three 150 W xenon lamps (wavelength > 420 nm), T = 303 K, stirring rate = 1000 rpm, reaction time = 3 h. The attached is the activities for phenol degradation under UV irradiation. Reaction conditions: 0.050 g catalyst, 30 ml 0.050 g/l phenol, reaction time = 2 h, three 6 W lamps (characteristic wavelength = 254 nm) located at 4 cm above the reaction solution.

of calcination temperature (Figure S10). The activity increases with the calcination temperature up to 773 K owing to the enhanced crystallization degree of anatase. Further increase in calcination temperature results in lower activity due to the decrease in S_{BET} and even the phase transformation from anatase to rutile [47]. Meanwhile, the activity of $La_2O_3/Ti_{1-x}B_xO_2$(SC) calcined at 773 K depends strongly on the B-content (Figure S11). The maximum activity is obtained on the $La_2O_3/Ti_{1-x}B_xO_2$(SC)-4 with the B/Ti molar ratio of 2.2%. Besides the enhanced S_{BET}, the promoting effect from B-doping could be mainly attributed to formation of the Ti–O–B bond which decreases E_g owing to the appearance of intermediate energy levels, leading to strong absorbance for visible lights. Meanwhile, the B-doping also increases the oxygen vacancies and/or crystal defects which could capture photoelectrons and thus, inhibit the recombination between the photoelectrons and holes, leading to the higher quantum efficiency. However, very high B-content is harmful for the activity due to the formation of B_2O_3 separate phase which may cover the active sites for in the $La_2O_3/Ti_{1-x}B_xO_2$(SC).

Fig. 5 demonstrates that only the B-doped TiO_2 samples display activity in visible region. However, the TiO_2(DC), TiO_2(SC) and the La_2O_3/TiO_2(SC) samples display very poor activity since these catalysts could not be activated by visible lights due to the big band gaps (3.2 eV). The $La_2O_3/Ti_{1-x}B_xO_2$(SC)-4 is more active than either the $Ti_{1-x}B_xO_2$(SC) O_2(SC) or the corresponding $La_2O_3/Ti_{1-x}B_xO_2$(DC) with the same B/Ti and La/Ti molar ratios, indicating that both the La_2O_3 and the supercritical treatment promote the photocatalysis, which is further confirmed by the attached activity diagram obtained from photocatalytic degradation of phenol under irradiation with 254 nm UV light. Besides higher S_{BET}, the promoting effect of supercritical treatment could be mainly attributed to higher crystallization of anatase and more surface oxygen vacancies and/or crystal defects [18], which could inhibit the recombination between photoelectrons and holes [27–30], leading to higher quantum efficiency. In addition, the supercritical treatment could ensure the incorporation of the B-dopants into the TiO_2 lattice to form Ti–O–B bonds and also strengthen the interaction between the B-dopants and the TiO_2, resulting in a narrower energy band gap and thus, the $La_2O_3/Ti_{1-x}B_xO_2$(SC) is easier to be activated by visible lights than the $La_2O_3/Ti_{1-x}B_xO_2$(DC). The presence of La_2O_3 could enhance S_{BET}, stabilize anatase against phase change, and also inhibit the photoelectron–hole recombination via trapping photoelectrons [32], leading to higher quantum efficiency. Although the La_2O_3/TiO_2(SC) is inactive in visible area, it exhibits even higher activity than the $Ti_{1-x}B_xO_2$(SC) during photocatalytic reaction under UV light irradiation owing to the enhanced UV light absorbance efficiency (see Fig. 4). The $La_2O_3/Ti_{1-x}B_xO_2$(SC)-4 exhibits much higher activity than the P25 TiO_2 under irradiation with either the UV lights or visible lights, which could be attributed to the promoting effects from both the La_2O_3 and the B-dopant. Meanwhile, the $La_2O_3/Ti_{1-x}B_xO_2$(SC)-4 could be used repetitively for more than 10 times without significant decline in the activity (see Figure S12), showing a good potential in practical application.

In summary, a new approach has been developed to synthesize the $La_2O_3/Ti_{1-x}B_xO_2$ photocatalyst under supercritical conditions. The as-prepared $La_2O_3/Ti_{1-x}B_xO_2$ exhibits high activity in photocatalytic degradation owing to synergetic promoting effects from both the La_2O_3 and the B-dopant as well as the supercritical treatment. Based on the present method, other doped TiO_2 visible photocatalysts and even non-titanium visible photocatalysts could be synthesized, which offers more opportunities for practical application of photocatalysis in environmental cleaning.

Acknowledgments

This work was supported by the Science and Technology ministry of China (2005CCA01100), Shanghai Science and Technology ministry (065412070), Shanghai Leading Academic Discipline Project (T0402), and Shanghai Municipal Education Commission (06DZ013).

Appendix A. Supplementary data

Supplementary data associated with this article can be found, in the online version, at doi:10.1016/j.apcatb.2008.02.005.

References

[1] A. Fujishima, T.N. Rao, D.A. Tryk, J. Photochem. Photobiol. C 1 (2000) 1.
[2] J.M. Hermana, C. Guillard, J. Disdier, C. Lehaut, S. Maitao, J. Blanco, Appl. Catal. B 35 (2002) 281.
[3] U.M.K. Shahed, A. Mofareh, B. William, J. Ingler, Science 297 (2002) 2243.
[4] S. Usseglio, A. Damin, D. Scarano, S. Bordiga, A. Zecchina, C. Lamberti, J. Am. Chem. Soc. 129 (2007) 2822.

[5] D. Zhang, J.A. Downing, F.J. Knorr, J.L. McHale, J. Phys. Chem. B 110 (2006) 21890.
[6] W.K. Choy, W. Chu, Ind. Eng. Chem. Res. 44 (2005) 8184.
[7] V.K. Gupta, R. Jain, A. Mittal, M. Mathur, S. Sikarwar, J. Colloid Interf. Sci. 309 (2007) 464.
[8] A. Dickinson, D. James, N. Perkins, T. Cassidy, M. Bowker, J. Mol. Catal. A 146 (1999) 211.
[9] H.X. Li, Z.F. Bian, J. Zhu, Y.N. Huo, H. Li, Y.F. Lu, J. Am. Chem. Soc. 129 (2007) 4538.
[10] X.Z. Li, F.B. Li, Environ. Sci. Technol. 35 (2001) 2381.
[11] C. Hu, Y.Q. Lan, J.H. Qu, X.X. Hu, A.M. Wang, J. Phys. Chem. B 110 (2006) 4066.
[12] B.M. Wen, C.Y. Liu, Y. Liu, Inorg. Chem. 44 (2005) 6503.
[13] R.J. Tayade, R.G. Kulkarni, R.V. Jasra, Ind. Eng. Chem. Res. 45 (2006) 5231.
[14] X.H. Wang, J.G. Li, H. Kamiyama, Y. Moriyoshi, T. Ishigaki, J. Phys. Chem. B 110 (2006) 6804.
[15] N. Venkatachalam, M. Palanichamy, B. Arabindoo, V. Murugesan, J. Mol. Catal. A 266 (2007) 158.
[16] S. Sakthivel, M. Janczarek, H. Kisch, J. Phys. Chem. B 108 (2004) 19384.
[17] E.A. Reyes-Garcia, Y.P. Sun, K. Reyes-Gil, D. Raftery, J. Phys. Chem. C 111 (2007) 2738.
[18] J.C. Yu, J.G. Yu, W.K. Ho, Z.T. Jiang, L.Z. Zhang, Chem. Mater. 14 (2002) 3808.
[19] S.K. Mohapatra, M. Misra, V.K. Mahajan, K.S. Raja, J. Phys. Chem. C 111 (2007) 8677.
[20] S. Ferrere, Chem. Mater. 12 (2000) 1083.
[21] V. Shklover, M.K. Nazeeruddin, S.M. Zakeeruddin, C. Barbe, A. Kay, T. Haibach, W. Steurer, R. Hermann, H.U. Nissen, M. Gratzel, Chem. Mater. 9 (1997) 430.
[22] S.M. Zakeeruddin, M.K. Nazeeruddin, R. Humphry-Baker, P. Pechy, P. Quagliotto, C. Barolo, G. Viscardi, M. Gratzel, Langmuir 18 (2002) 952.
[23] R. Ghanem, Y.H. Xu, J. Pan, T. Hoffmann, J. Andersson, T. Polıvka, T. Pascher, S. Styring, L.C. Sun, V. Sundstroim, Inorg. Chem. 41 (2002) 6258.
[24] W. Zhao, W.H. Ma, C.C. Chen, J.C. Zhao, Z.G. Shuai, J. Am. Chem. Soc. 126 (2004) 4782.
[25] Y. Cong, J.L. Zhang, F. Chen, M. Anpo, D.N. He, J. Phys. Chem. C 111 (2007) 10618.
[26] C.P. Sibu, K.S. Rajesh, P. Mukundan, K.G.K. Warrier, Chem. Mater. 14 (2002) 2876.
[27] H.X. Li, X.Y. Zhang, Y.N. Huo, J. Zhu, Environ. Sci. Technol. 41 (2007) 4410.
[28] H.X. Li, J.X. Li, Y.N. Huo, J. Phys. Chem. B 110 (2006) 1559.
[29] H.X. Li, G.S. Li, J. Zhu, Y. Wan, J. Mol. Catal. A 226 (2005) 93.
[30] H.X. Li, J. Zhu, G.S. Li, Chem. Lett. 33 (2004) 574.
[31] A.W. Xu, Y. Gao, H.Q. Liu, J. Catal. 207 (2002) 151.
[32] Y.N. Huo, J. Zhu, J.X. Li, G.S. Li, H.X. Li, J. Mol. Catal. A 278 (2007) 237.
[33] Operator's reference manual for PHI PC windows software Version 1.2b, Physical Electronic Division, Perkin-Elmer, p. 274.
[34] M. Mrowetz, W. Balcerski, A.J. Colussi, M.R. Hoffmann, J. Phys. Chem. B 108 (2004) 17269.
[35] Y.J. Wang, M. Trenary, Chem. Mater. 5 (1993) 199.
[36] H. Li, H.X. Li, J.F. Deng, Appl. Surf. Sci. 152 (1999) 25.
[37] K.Y. Jung, S.B. Park, S. Ihm, Appl. Catal. B 51 (2004) 239.
[38] A. Serret, M.V. Cabanas, R.M. Vallet, Chem. Mater. 12 (2000) 3836.
[39] T. Osaki, K. Nagashima, K. Watari, K. Tajiri, J. Non-Crystal. Solids 353 (2007) 2436.
[40] V. Gourinchas-Courtecuisse, F. Bocquet, K. Chhor, C. Pommier, J. Supercritical Fluids 9 (1996) 222.
[41] C. Aymonier, A. Loppinet-Serani, H. Reveron, Y. Garrabos, F. Cansell, J. Supercritical Fluids 38 (2006) 242.
[42] J. Zhu, J. Yang, Z.F. Bian, Y. Liu, J. Ren, Y. Cao, H.X. Li, W. Dai, H. He, K.N. Fan, Appl. Catal. B 76 (2007) 82.
[43] H. Yamashita, Y. Ichihashi, M. Anpo, J. Phys. Chem. 100 (1996) 16041.
[44] M. Yoon, M. Seo, C. Jeong, J.H. Jang, K.S. Jeon, Chem. Mater. 17 (2005) 6069.
[45] L. Li, Y. Yang, X. Huang, G. Li, L. Zhang, J. Phys. Chem. B 109 (2005) 12394.
[46] H. Fei, Y. Liu, Y. Li, P. Sun, Z. Yuan, B. Li, D. Ding, T. Chen, Microp. Mesop. Mater. 102 (2007) 318.
[47] J.A. Wang, R. Limas-Ballesteros, T. Lopez, A. Moreno, R. Gomez, O. Novaro, X. Bokhimi, J. Phys. Chem. B 105 (2001) 9692.